Check for updates

The preparation, characterization and catalytic activity of Ni NPs supported on porous alginate-*g*-poly(*p*-styrene sulfonamide-*co*-acrylamide)†

Sedigheh Alavinia and Ramin Ghorbani-Vaghei 🆔 *

Herein, we report the synthesis of nickel nanoparticles under mild conditions using porous alginate-*g*-poly(*p*-styrene sulfonamide-*co*-acrylamide) as a protecting/stabilizing agent and sodium borohydride as a reducing agent. The porous cross-linked polymeric support was prepared *via* combining the use of sol–gel, nanocasting, and crosslinking techniques, in which the *p*-styrene sulfonamide monomer (PSSA) and *N*,*N*′-methylene-bis (acrylamide) (MBA) cross-linker underwent copolymerization on the surface of sodium alginate in the presence of a SiO$_2$ nanoparticle (NP) template (Alg–PSSA-*co*-ACA). The prepared catalyst (Alg–PSSA-*co*-ACA@Ni) showed high catalytic activity for the one-step synthesis of 1,3,4-oxadiazoles from the reaction of hydrazides and aryl iodides through isocyanide insertion/cyclization.

1. Introduction

Oxadiazole and its fused derivatives represent a wide range of biological and pharmacological activities. In particular, 1,3,4-oxadiazoles are one of the most important antitumor drugs in clinical use today.[1] They represent the core structure of several antitumor and anti-HIV drugs on the market, including zibotentan,[2] and raltegravir.[3] Hence, some methods have recently been reported for the synthesis of 1,3,4-oxadiazoles, such as the annulation of methyl ketones or acyl chlorides with hydrazides,[4] the cyclization of 1,2-diacylhydrazines,[5] the cyclization of acyl-hydrazones,[6] imine C–H bond activation of *N*-arylidenear-oylhydrazide,[7] arylation of the 1,3,4-oxadiazoles,[8] intramolecular decarboxylation,[9] and the isocyanide insertion reaction.[10] However, some of these require harsh reaction conditions, and expensive noble and precious metal-based catalyst systems which results in increased production costs owing to the difficulty in separating the desired products. Thus, it is of great significance to develop a novel catalytic system, which can afford the functionalized 1,3,4-oxadiazoles in excellent yields under mild reaction conditions using a heterogeneous support.

Porous polymers have been widely studied as solid supports owing to their high specific surface area and excellent thermal stability. Porous polymers with an appropriate chemical composition allow the fabrication of materials that are both biocompatible and have a uniform porosity.[11–14] In order to precisely control the pore size, the synthesis of mesoporous polymers from silica nanoparticles (NPs) using the nanocasting route is a practical and efficient technique.[15,16] Although the synthesis of porous polymers has been widely investigated, there is still a lack of practical procedures to prepare mesoporous natural polysaccharides with high chemical and thermal stabilities. Here, a sodium alginate-based polymer with a mesoporous structure was synthesized as a heterogeneous support for the immobilization of Ni NPs.

Sodium alginate is a member of the natural polysaccharides. Owing to its potential to transform into different forms (such as gels, spheres, and fibres), and its non-toxic and eco-friendly nature, it is used as a powerful heterogeneous catalyst. Other factors that play an important role in the catalytic performance of sodium alginate are its biodegradable, biocompatible and abundant nature.[17–22] In order to improve the catalytic activity of sodium alginate, specific methods have been proposed, such as blending polymers,[23] compounding with natural and synthetic chemical derivatives,[24] and grafting copolymerization with vinyl monomers.[25–27]

Sulfonamide scaffolds have attracted remarkable attention owing to their potential application in medicinal,[28] and catalytic activity.[29] The results obtained from the catalytic application of sulfonamides indicate that sulfonamides play a vital role in heterogeneous substrates and catalysts.[29] Owing to the biomedical and catalytic application of sulfonamides, *p*-styrene sulfonamide can be considered as a promising candidate for the synthesis of sodium alginate based catalysts using graft copolymerization. Similarly, by grafting of PSSA and cross-linking of *N*,*N*′-methylene-bis(acrylamide) with alginate through the nanocasting route a novel type of porous polymer was synthesized. By modifying the chemically active sites and mesoporous structure of Alg–PSSA-*co*-ACA, it can be used as

*Department of Chemistry, Bu-Ali Sina University, 65174, Hamedan, Iran. E-mail: rgvaghei@yahoo.com; Tel: +98 81 38380647

† Electronic supplementary information (ESI) available: Detailed experimental procedure and FT-IR and MS analysis of all compounds. See DOI: 10.1039/d1ra04022g
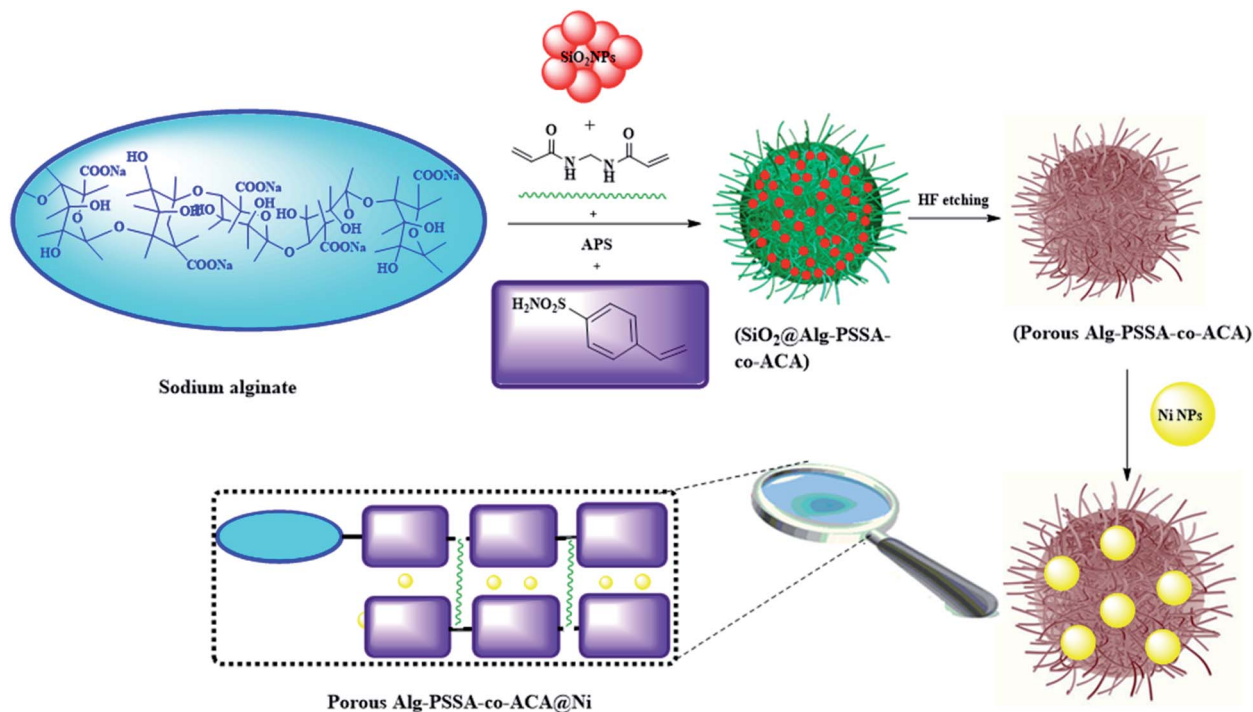
Scheme 1 A schematic diagram of the preparation of SiO$_2$@Alg–PSSA-*co*-ACA, porous Alg–PSSA-*co*-ACA, and porous Alg–PSSA-*co*-ACA@Ni (APS: ammonium persulfate).

a novel amphiphilic support for the immobilization of Ni NPs (Scheme 1).

Therefore, some specific methods used to improve the catalytic performance of porous alginate-*g*-poly (*p*-styrene sulfonamide-*co*-acrylamide) are: (i) creating a mesoporous structure in the alginate-*g*-poly (*p*-styrene sulfonamide-*co*-acrylamide). This mesoporous structure allows the reactants and Ni NPs to rapidly diffuse through the mesopores, and enables the formation of a large surface area; (ii) the addition of PSSA in the catalyst formulation could have promising advantages, including: (a) a high chemical and thermal stability under the reaction conditions,[30] and (b) the amphiphilic properties of the catalyst;[29d] and (iii) the interaction of Ni NPs with PSSA can decrease the self-aggregation and leaching of Ni NPs.[31]

Following on from our recent work on the design and application of a multifunctional sulfonamide-based catalyst,[29,32] and the synthesis of functionalized oxadiazole,[29d] in this article, we herein report the green synthesis of 1,3,4-oxadiazoles from the reaction of hydrazides, aryl iodides and *tert*-butyl isocyanide in the presence of an Alg–PSSA-*co*-ACA@Ni catalyst (Scheme 2). The prepared porous nanocomposite revealed an excellent

catalytic functionality for the synthesis of different 1,3,4-oxadiazoles with high yields.

2. Experimental

2.1. Synthesis of silica alginate-*g*-poly(*p*-styrene sulfonamide-*co*-acrylamide) (SiO$_2$@Alg–PSSA-*co*-ACA)

The silica NPs were synthesized using the Stöber method.[33] Then, the mixture of *p*-styrene sulfonamide (1.5 g), MBA (0.2 g) and SiO$_2$ NPs (0.05 g) was gradually added to the sodium alginate solution (0.5 g in 20 mL distilled water). Finally, ammonium persulfate (APS) (0.6 g) was added and the mixture was stirred at 60 °C for 2 h. The synthesized SiO$_2$@Alg–PSSA-*co*-ACA nanocomposite, in the form of a gel, was dried at room temperature (weight: 5 g).

2.2. Synthesis of porous alginate-*g*-poly(styrene sulfonamide-*co*-acrylamide) (Alg–PSSA-*co*-ACA)

In order to synthesize the mesoporous structure, SiO$_2$ NPs of SiO$_2$@Alg–PSSA-*co*-ACA were selectively removed through etching the silica NPs by mixing a HF solution (5 mL, 10 wt%)
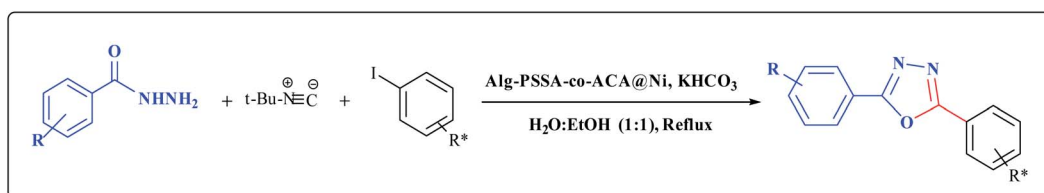
Scheme 2 The synthesis of 1,3,4-oxadiazole derivatives using Alg–PSSA-*co*-ACA@Ni in the presence of H$_2$O : EtOH and KHCO$_3$.

with a solution of SiO$_2$@Alg–PSSA-*co*-ACA (1 g in 20 mL deionized water) in a plastic tube. The prepared solution was stirred for 3 h. The resultant porous Alg–PSSA-*co*-ACA was separated by filtration, washed with water, and dried (weight: 0.85 g).

2.3. Nickel NPs immobilized on porous alginate-*g*-poly(*p*-styrene sulfonamide-*co*-acrylamide) (Alg–PSSA-*co*-ACA@Ni)

To synthesize the Alg–PSSA-*co*-ACA@Ni, the obtained porous Alg–PSSA-*co*-ACA (0.1 g) in a solution of NiCl$_2$·6H$_2$O (1 M, 5 mL) was stirred at room temperature for 2 h, then the solution of NaBH$_4$ (10 mmol in 5 mL ethanol) was slowly added and stirred at room temperature for 60 min. The functionalized Alg–PSSA-*co*-ACA@Ni was separated using centrifugation, washed with distilled water (3 × 20 mL), and dried under a vacuum at room temperature for 12 h (weight: 0.3 g) (Scheme 1).[34] The amount of Ni incorporated in the support was 1.6 mmol g^{-1}, as corroborated using inductively coupled plasma optical emission spectroscopy (ICP-OES).

2.4. General procedure for the synthesis of the 1,3,4-oxadiazoles

A mixture of substituted benzohydrazide (1 mmol), substituted aryl iodide (1 mmol), KHCO$_3$ (1 mmol), *tert*-butyl isocyanide (1.5 mmol), and Alg–PSSA-*co*-ACA@Ni (1.5 mol%, 9 mg) was refluxed in H$_2$O : EtOH (2 mL, 1 : 1). After completion of the reaction (monitored using TLC, *n*-hexane/ethyl acetate, 10 : 4), the catalyst was separated from the reaction mixture by centrifugation and washed with ethanol (10 mL). Finally, the solvent was evaporated and the solid obtained was crystallized from ethanol (10 mL). In some cases, the residue was purified using a short silica gel column using *n*-hexane/ethylacetate (10 : 4).

2.5. Spectral data for the compounds

2-(2-Bromophenyl)-5-phenyl-1,3,4-oxadiazole. Mp 145–147 °C, ^{1}H NMR (500 MHz, CDCl$_3$-*d*$_3$) δ 6.83 (d, 2H, *J* = 8 Hz), 6.94 (t, 1H, *J* = 7.2 Hz), 7.30 (dd, 3H, *J* = 7.6, 5.6 Hz), 7.45 (t, 1H, *J* = 7.6 Hz), 7.69 (d, 1H, *J* = 7.6 Hz), 7.80 (dd, 1H, *J* = 6.4, 1.2 Hz). ^{13}C NMR (125 MHz, DMSO-*d*$_6$) δ 164.7, 163.2, 135.1, 132.6, 132.4, 132.1, 129.8, 129.4, 127.2, 127.1, 126.1, 123.6, 122.9. MS *m/z*: 299.1.

2.5.2 2-(2-Chlorophenyl)-5-(pyridin-4-yl)-1,3,4-oxadiazole. Mp 128–130 °C, ^{1}H NMR (500 MHz, DMSO-*d*$_6$) δ 8.85 (d, *J* = 4.8 Hz, 1H), 8.16 (d, *J* = 2.8 Hz, 1H), 8.12–8.03 (m, 2H), 7.87 (d, *J* = 5.5 Hz, 1H), 7.72 (dd, *J* = 8.1, 2.4 Hz, 1H), 7.65 (qd, *J* = 8.0, 7.5, 2.7 Hz, 1H), 7.51 (td, *J* = 8.0, 3.1 Hz, 1H). ^{13}C NMR (125 MHz, DMSO-*d*$_6$) δ 164.1, 163.3, 151.3, 134.6, 133.7, 133.3, 132.6, 131.9, 131.0, 130.7, 129.2, 128.3, 126.9, 126.0, 125.4, 120.8, MS *m/z*: 257.1.

2-(5-Phenyl-1,3,4-oxadiazol-2-yl) benzaldehyde. Mp 180–181 °C; ^{1}H NMR (500 MHz, DMSO-*d*$_6$) δ 6.85 (d, 2H, *J* = 8.4 Hz), 7.19 (t, 2H, *J* = 7.6 Hz), 7.44 (d, 1H, *J* = 4.8 Hz), 7.49 (dd, 2H, *J* = 7.6, 7.2 Hz), 7.61 (d, 2H, *J* = 7.2 Hz); 8.88 (s, 1H). ^{13}C NMR (125 MHz, DMSO-*d*$_6$) δ, 169.2, 160.1, 147.4, 146.8, 138.7, 134.8, 134.7, 134.1, 132.3, 132.2, 130.8, 130.4, 129.5, 128.0, 127.6, 127.2, 125.8, 125.0, 124.8, 124.5, 124.4, 124.1, 122.7. MS *m/z*: 250.07.

2-(3-Chlorophenyl)-5-(pyridin-4-yl)-1,3,4-oxadiazole. Mp 143–145 °C; ^{1}H NMR (250 MHz, DMSO-*d*$_6$) δ 8.85 (s, 2H), 8.19 (s, 1H), 8.10 (s, 3H), 7.69 (dq, *J* = 14.7, 7.7 Hz, 2H). ^{13}C NMR (63 MHz, DMSO-*d*$_6$) δ 164.1, 163.2, 151.3, 134.5, 132.6, 131.9, 130.7, 126.9, 126.0, 125.3, 121.0. MS *m/z*: 257.6.

2-Benzyl-5-phenyl-1,3,4-oxadiazole. Mp 102–103 °C; ^{1}H NMR (250 MHz, DMSO-*d*$_6$) δ 7.93 (d, *J* = 6.9 Hz, 2H), 7.56 (d, *J* = 6.2 Hz, 4H), 7.36 (d, *J* = 4.4 Hz, 4H), 4.34 (s, 2H). ^{13}C NMR (63 MHz, DMSO-*d*$_6$) δ 165.9, 164.6, 134.8, 132.2, 129.7, 129.2, 127.6, 126.7, 123.7, 31.2. MS *m/z*: 236.2.

2-(4-Bromophenyl)-5-phenyl-1,3,4-oxadiazole. Mp 165–166 °C; ^{1}H NMR (250 MHz, DMSO-*d*$_6$) δ 8.18–7.97 (m, 3H), 7.83 (d, *J* = 7.2 Hz, 3H), 7.71–7.55 (m, 3H). ^{13}C NMR (63 MHz, DMSO-*d*$_6$) δ 164.8, 163.8, 132.9, 132.5, 129.8, 129.0, 127.7, 126.1, 123.6, 122.9.

4-(5-Phenyl-1,3,4-oxadiazol-2-yl) aniline. Mp 191–193 °C; ^{1}H NMR (250 MHz, DMSO-*d*$_6$) δ 8.18–7.98 (m, 2H), 7.75 (d, *J* = 8.2 Hz, 2H), 7.58 (s, 3H), 6.69 (d, *J* = 8.2 Hz, 2H), 5.98 (s, 1H). ^{13}C NMR (63 MHz, DMSO) δ 165.2, 163.0, 152.9, 131.9, 129.7, 128.9, 128.6, 127.9, 126.7, 124.1, 114.0, 110.0. MS *m/z*: 237.2.

2-Benzyl-5-(*p*-tolyl)-1,3,4-oxadiazole. Mp 93–94 °C; ^{1}H NMR (250 MHz, DMSO-*d*$_6$) δ 7.79 (d, *J* = 7.8 Hz, 2H), 7.61–6.96 (m, 7H), 4.31 (s, 2H), 2.48 (s, 3H). ^{13}C NMR (63 MHz, DMSO-*d*$_6$) δ 165.6, 164.7, 142.3, 136.2, 134.9, 130.3, 129.7, 129.5, 129.3, 129.1, 128.6, 127.9, 127.6, 126.9, 126.7, 121.0, 31.2, 21.4.

2-Phenyl-5-(pyridin-4-yl)-1,3,4-oxadiazole. Mp 139–140 °C; ^{1}H NMR (250 MHz, DMSO-*d*$_6$) δ 8.83 (s, 2H), 8.13 (d, *J* = 6.5 Hz, 2H), 8.03 (d, *J* = 5.0 Hz, 2H), 7.62 (d, *J* = 9.2 Hz, 3H). ^{13}C NMR (63 MHz, DMSO-*d*$_6$) δ 165.2, 162.9, 151.3, 132.8, 130.9, 129.9, 127.3, 123.4, 120.7. MS *m/z*: 223.2.

2-(4-Chlorophenyl)-5-(pyridin-4-yl)-1,3,4-oxadiazole. Mp 140–143 °C; ^{1}H NMR (250 MHz, DMSO-*d*$_6$) δ 8.14 (d, *J* = 8.8 Hz, 4H), 7.70 (d, *J* = 7.5 Hz, 2H), 7.62–7.48 (d, *J* = 8 Hz, 2H), 2.42 (s, 3H). MS *m/z*: 257.04.

2-(Pyridin-4-yl)-5-(*p*-tolyl)-1,3,4-oxadiazole. Mp 140–142 °C; ^{1}H NMR (500 MHz, DMSO-*d*$_6$) δ 8.13 (d, *J* = 5 Hz, 2H), 8.04–8.00 (d, *J* = 2.5 Hz, 2H), 7.64 (d, *J* = 5 Hz, 2H), 7.44 (d, *J* = 7.9 Hz, 2H), 2.42 (s, 3H). ^{13}C NMR (125 MHz, DMSO-*d*$_6$) δ 164.5, 164.2, 142.6, 132.4, 130.4, 130.4, 129.8, 127.1, 127.0, 123.8, 121.0, 21.6. MS *m/z*: 237.2.

2-(2-Chlorophenyl)-5-phenyl-1,3,4-oxadiazole. Mp 96–98 °C; ^{1}H NMR (250 MHz, DMSO-*d*$_6$) δ 8.10 (ddt, *J* = 7.9, 4.6, 1.4 Hz, 3H), 7.73 (dt, *J* = 7.9, 1.3 Hz, 1H), 7.70–7.52 (m, 5H). ^{13}C NMR (125 MHz, DMSO-*d*$_6$) δ ^{13}C NMR (63 MHz, DMSO) δ 133.7, 132.7, 131.8, 131.6, 129.9, 128.3, 127.2, 123.5. MS *m/z*: 257.6.

4-(5-Phenyl-1,3,4-oxadiazol-2-yl) benzoic acid. Mp 217–218 °C; ^{1}H NMR (500 MHz, DMSO-*d*$_6$) δ 12.6 (s, 1H), 8.34 (s, 1H), 8.24 (d, *J* = 8.0 Hz, 1H), 8.19–8.09 (m, 4H), 7.64 (d, *J* = 10 Hz, 3H). ^{13}C NMR (126 MHz, DMSO-*d*$_6$) δ 166.9, 164.8, 163.9, 134.0, 132.6, 132.5, 130.6, 129.9, 129.8, 129.6, 128.0, 127.4, 127.3, 127.2, 127.1, 123.6. MS *m/z*: 266.6.

2-(4-Bromophenyl)-5-(3-methoxyphenyl)-1,3,4-oxadiazole. Mp 152–153 °C, ^{1}H NMR (400 MHz, DMSO-*d*$_6$) δ 8.06 (d, *J* = 8.0 Hz, 2H), 7.82 (d, *J* = 8.0 Hz, 2H), 7.70 (d, *J* = 8.0 Hz, 1H), 7.60 (s, 1H), 7.54 (t, *J* = 7.7 Hz, 1H), 7.21 (dd, *J* = 8, 4 Hz, 1H), 3.89 (s, 3H). ^{13}C NMR (100 MHz, DMSO-*d*$_6$) δ 164.5, 164.4, 160.0, 132.6,

131.2, 129.8, 127.1, 124.6, 123.4, 119.4, 118.5, 111.9, 111.8, 55.8. MS m/z: 330.0.

2,5-Diphenyl-1,3,4-oxadiazole. Mp 132–133 °C; ^{1}H NMR (400 MHz, DMSO-d_6) δ 8.12 (dd, $J = 8$, 4 Hz, 4H), 7.63 (m, 6H), ^{13}C NMR (101 MHz, DMSO) δ 164.6, 132.6, 129.9, 127.1, 123.5.

2-(4-Bromophenyl)-5-(p-tolyl)-1,3,4-oxadiazole. Mp 200–202 °C; ^{1}H NMR (400 MHz, DMSO-d_6) δ 8.06 (d, $J = 8.4$ Hz, 2H), 8.01 (d, $J = 8$ Hz, 1H), 7.83 (d, $J = 6$ Hz, 2H), 7.65 (d, $J = 8.4$ Hz, 1H), 7.44 (d, $J = 8$ Hz, 2H), 2.49 (s, 3H). MS m/z: 315.0.

2-Phenyl-5-(p-tolyl)-1,3,4-oxadiazole. Mp 122–124 °C; ^{1}H NMR (400 MHz, DMSO-d_6) δ 8.13–8.10 (m, 3H), 8.06 (d, $J = 9.6$ Hz, 1H), 7.82 (d, $J = 8$ Hz, 1H), 7.64 (t, $J = 6.4$ Hz, 4H), 2.51 (s, 3H). ^{13}C NMR (100 MHz, DMSO-d_6) δ 164.6, 163.8, 132.9, 132.0, 129.8, 129.0, 127.1, 126.1, 123.7, 123.0, 23.2. m/z: 236.

2-(3-Methoxyphenyl)-5-phenyl-1,3,4-oxadiazole. Mp 148–149 °C; ^{1}H NMR (400 MHz, DMSO-d_6) δ 8.09 (dd, 3.2, 1.2 Hz, 2H), 7.66 (dd, $J = 7.7$, 1.3 Hz, 1H), 7.64–7.59 (m, 3H), 7.56 (t, $J = 1.6$ Hz, 1H), 7.51 (t, $J = 8.0$ Hz, 1H), 7.21 (dd, 4.0, 2.8 Hz, 1H), 3.82 (s, 3H). ^{13}C NMR (100 MHz, DMSO-d_6) δ 164.5, 164.4, 160.0, 132.6, 131.2, 129.8, 127.1, 124.6, 123.4, 119.4, 118.5, 111.9, 111.8, 55.8. m/z: 252.2.

2-(4-Bromophenyl)-5-(pyridin-4-yl)-1,3,4-oxadiazole. Mp 180 °C; ^{1}H NMR (400 MHz, DMSO-d_6) δ 8.83 (d, $J = 5.8$ Hz, 2H), 8.08 (dd, $J = 10.0$, 7.3 Hz, 4H), 7.84 (d, $J = 8.5$ Hz, 2H). ^{13}C NMR (101 MHz, DMSO-d_6) δ 151.2, 133.0, 129.3, 120.9. m/z: 300.1.

2-(2,3-Dichlorophenyl)-5-phenyl-1,3,4-oxadiazole. Mp 146–147 °C; ^{1}H NMR (400 MHz, DMSO-d_6) δ 8.51 (ddd, $J = 7.8$, 6.7, 1.4 Hz, 2H), 8.29 (t, $J = 7.9$ Hz, 2H), 7.96 (t, $J = 7.8$ Hz, 2H), 7.57 (dd, $J = 2$, 1.2 Hz, 2H), 7.49 (t, $J = 7.6$ Hz, 1H). ^{13}C NMR (100 MHz, DMSO) δ 155.5, 134.6, 132.6, 131.2, 129.1, 128.7, 127.9, 118.6, 118.5, 118.3.

2-(2-Methoxyphenyl)-5-phenyl-1,3,4-oxadiazole. Mp 118–120 °C; ^{1}H NMR (400 MHz, DMSO-d_6) δ 7.60 (d, $J = 6.4$ Hz, 2H), 7.44 (t, $J = 7.8$ Hz, 2H), 7.20 (t, $J = 7.8$ Hz, 2H), 7.13 (d, $J = 8.3$ Hz, 1H), 7.07 (t, $J = 7.5$ Hz, 1H), 6.74 (t, $J = 7.3$ Hz, 1H), 3.87 (s, 3H). ^{13}C NMR (101 MHz, DMSO) δ 156.4, 145.9, 130.5, 129.0, 128.4, 120.6, 119.3, 118.1, 113.6, 113.6, 111.5, 55.7.

2-(4-Fluorophenyl)-5-phenyl-1,3,4-oxadiazole. Mp 150–151 °C; ^{1}H NMR (400 MHz, DMSO-d_6) δ 8.64 (t, $J = 5.6$ Hz, 2H), 8.33 (t, $J = 8.7$ Hz, 2H), 8.19 (t, $J = 7.7$ Hz, 2H), 7.84 (d, $J = 7.9$ Hz, 1H), 7.75 (t, $J = 7.3$ Hz, 1H), 7.70 (d, $J = 9.6$ Hz, 1H). ^{13}C NMR (101 MHz, DMSO-d_6) δ 163.3, 160.9, 145.7, 129.0, 119.4, 116.4, 115.9, 115.6, 113.8.

3. Results and discussion

3.1. Characterization of the catalyst

The synthesized Alg–PSSA-co-ACA@Ni catalyst was fully characterized using Fourier transform infrared spectroscopy (FT-IR), thermogravimetric analysis (TGA), inductively coupled plasma mass spectrometry (ICP-MS), field emission scanning electron microscopy with energy dispersive X-ray spectroscopy (FESEM-EDX) mapping techniques and N_2 isotherms. The FT-IR spectrum of sodium alginate, SiO_2@Alg–PSSA-co-ACA, mesoporous

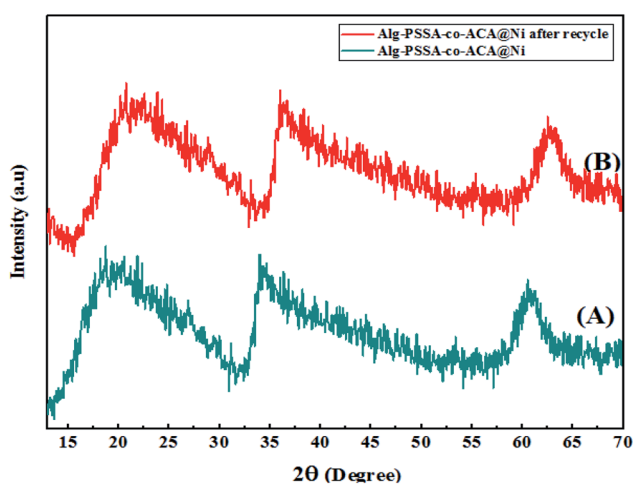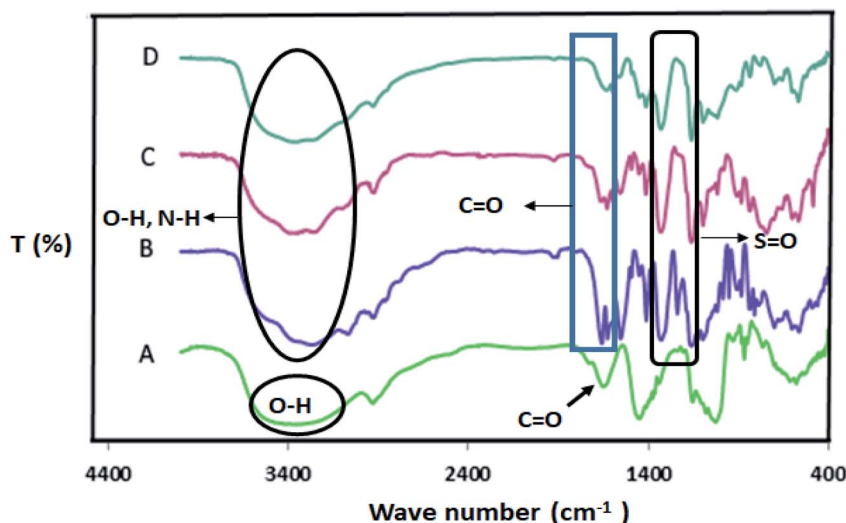**Fig. 2** XRD patterns of porous Alg–PSSA-co-ACA@Ni before (A) and after (B) the reaction.

Fig. 1 FT-IR spectra of NaAlg (A), SiO_2@Alg–PBSA-co-ACA (B), porous Alg–PSSA-co-ACA (C), and Alg–PSSA-co-ACA@Ni (D).
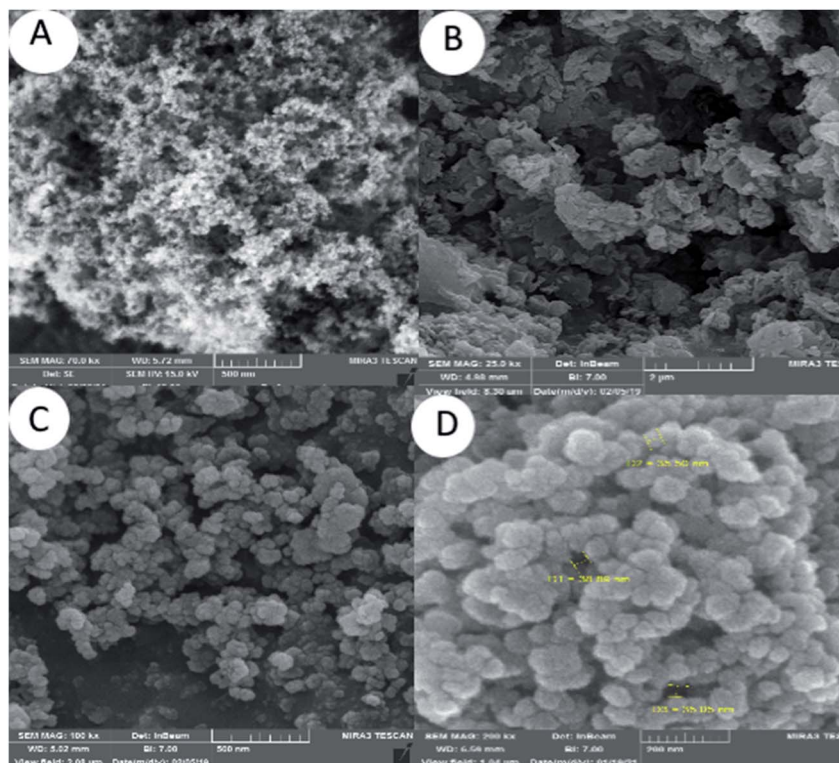
Fig. 3 FE-SEM photographs of SiO$_2$NPs (A), mesoporous Alg–PSSA-*co*-ACA (B), and mesoporous Alg–PSSA-*co*-ACA@Ni (C and D).

Alg–PSSA-*co*-ACA, and Alg–PSSA-*co*-ACA@Ni is shown in Fig. 1. The results obtained from the FT-IR spectrum show: (i) the presence of the SiO$_2$ NPs template; (ii) the polymerization of PSSA and crosslinking of the MBA groups; (iii) the selective removal of the SiO$_2$ NPs from SiO$_2$@Alg–PSSA-*co*-ACA; and (iv) the interaction of Ni NPs with the prepared support. The FT-IR spectrum of NaAlg displayed vibrational bands at 1642 and 1454 cm^{-1} (representing the vibrations of the carboxylate anions). The vibrational bands at 3412 and 2929.87 cm^{-1} can be attributed to the O–H and C–H stretching, respectively

(Fig. 1A).[17] The FT-IR spectrum of SiO$_2$@Alg–PSSA-*co*-ACA displayed new bands at 3363, 3090 and 1662 cm^{-1} that can be attributed to the O–H, C–H and C=O amide stretching bands, respectively. The presence of these peaks confirmed the successful crosslinking of MBA. In addition, the presence of new bands at 1328 and 1159 cm^{-1} (owing to the O=S=O stretching) confirmed the successful polymerization of PSSA.[35] Also, the peaks at 1180 cm^{-1} proved the presence of the SiO$_2$ NPs (Fig. 1B).[36] After the silica etching procedure, this peak was not observed in the FT-IR spectra of the porous Alg–PSSA-*co*-
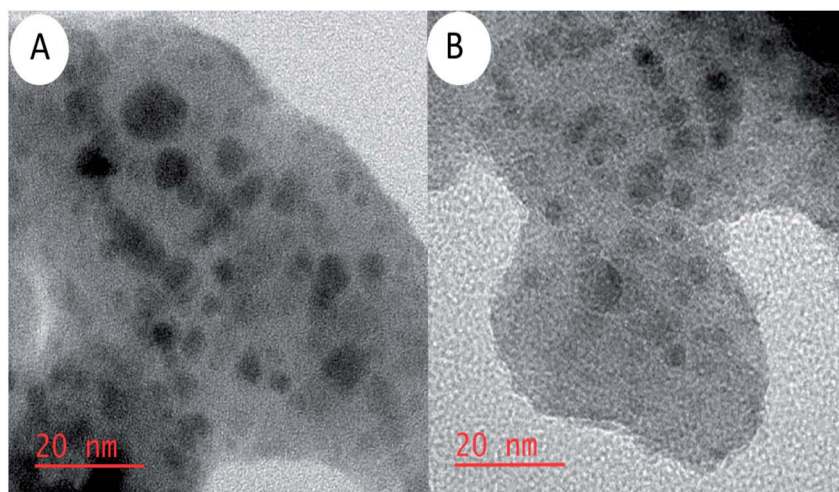

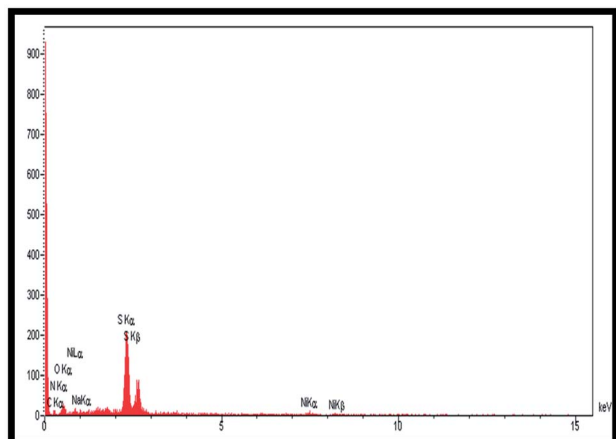**Fig. 4** HR-TEM photographs of mesoporous Alg–PSSA-*co*-ACA@Ni before (A) and after (B) the reaction.

© 2021 The Author(s). Published by the Royal Society of Chemistry

Fig. 5   The EDX spectrum of Alg–PSSA-*co*-ACA@Ni.

Table 1   Elemental percentages of Alg–PSSA-*co*-ACA@Ni

Element	W%	A%
C	28.34	42.36
N	9.28	6.76
O	26.10	29.28
Na	1.13	0.88
S	30.41	19.27
Ni	4.74	1.45
Total	100.0	

ACA and Alg–PBSA-*co*-ACA@Ni (Fig. 1C and D). In the FT-IR spectrum of Alg–PSSA-*co*-ACA@Ni (Fig. 1D), after interaction of the Ni NPs with the prepared support, the band at 3392 cm^{-1} (resulting from the NH_2 stretching, Fig. 3C) shifted to lower wave number (3363 cm^{-1}). In addition, the amide peaks shifted from 1633 to 1600 cm^{-1}. Based on the strong co-ordination of

the Ni NPs with the composite, the IR absorption peaks of the organo-functions are slightly shifted to the lower region.

Fig. 2 shows the X-ray diffraction pattern of the porous Alg–PSSA-*co*-ACA@Ni samples before (Fig. 2A) and after the reaction (Fig. 2B). Comparison of X-ray diffractometry (XRD) patterns of the Alg–PSSA-*co*-ACA@Ni sample shows that the structure of the prepared catalyst did not changed significantly after the reaction. The diffraction peaks appeared at $2\theta = 60°$ and can be attributed to the Ni NPs.[37] Meanwhile, in the XRD pattern of the Alg–PSSA-*co*-ACA@Ni nanocomposite sample, an amorphous phase is observed, which is related to the presence of amorphous polymer filaments of acrylamide ($2\theta = 20–30$ degrees),[38] and sodium alginate ($2\theta = 35–40$ degrees),[39] and polystyrene sulfonamide ($2\theta = 20–30$ degrees).[40] It is worth noting that the crystal structure of the recovered catalyst sample is quite similar to that of the original catalyst structure and the peak positions of the peaks have only changed a little, indicating the stability of the recovered catalyst. Therefore, the prepared catalyst can be reused several times after a simple recovery period.

The morphology of the SiO_2 NPs, mesoporous Alg–PSSA-*co*-ACA and Alg–PSSA-*co*-ACA@Ni was characterized using FE-SEM analysis (Fig. 3). The FE-SEM images of the spherical SiO_2 NPs showed a uniform distribution (Fig. 3A). The FE-SEM image of Alg–PSSA-*co*-ACA obtained using the silica template method demonstrated the mesoporous structure of the Alg–PSSA-*co*-ACA (Fig. 3B). Fig. 3B shows the rough morphology of the surface, which results in the increased activity of the catalyst. Fig. 3C and D show the distribution of the spherically shaped Ni particles on the surface of the mesoporous Alg–PSSA-*co*-ACA.

The high-resolution transmission electron microscopy (HR-TEM) images of the Alg–PSSA-*co*-ACA@Ni (Fig. 4A) and the recovered catalyst (Fig. 4B) are depicted in Fig. 4. The HR-TEM images showed that the sample has uniform particles that are approximately 20 nm in size. The good dispersion of the Ni species was visible at higher magnifications in the HR-TEM image, a very thin layer of the porous polymer could be
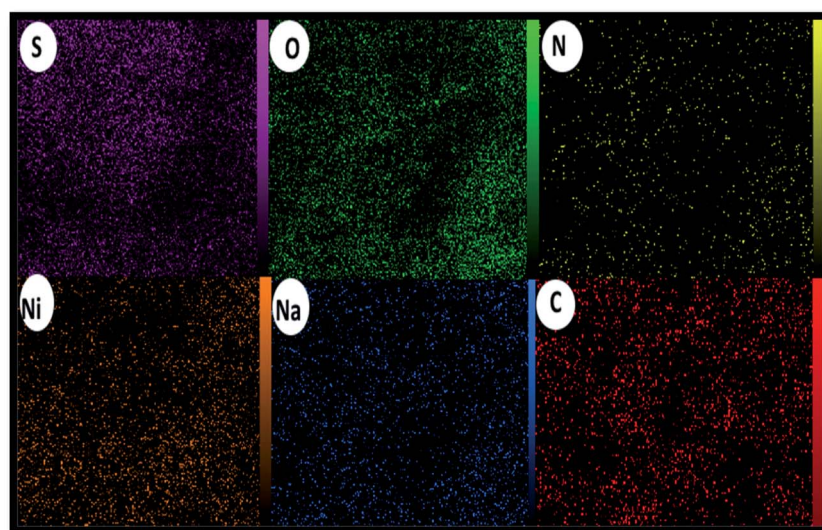

Fig. 6   Elemental mapping of C, N, O, S, Ni, and Na atoms achieved from the SEM micrographs.
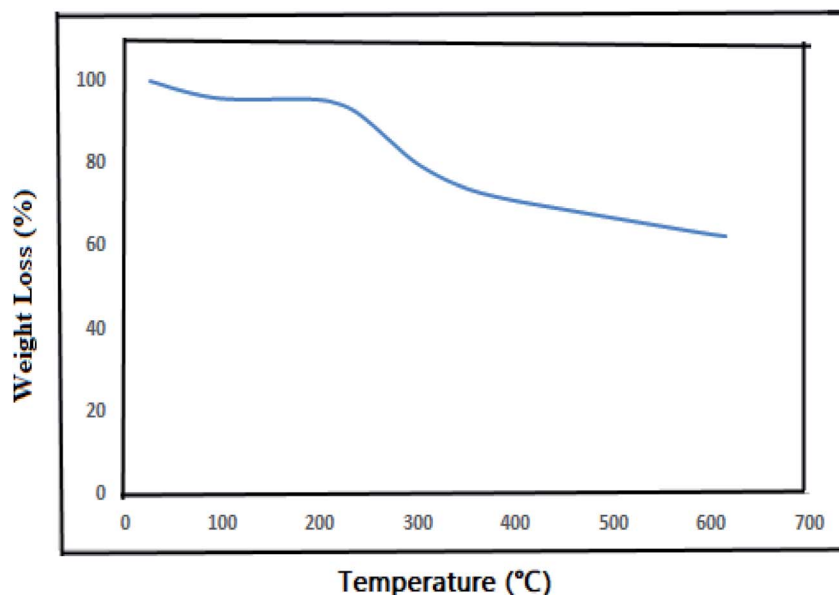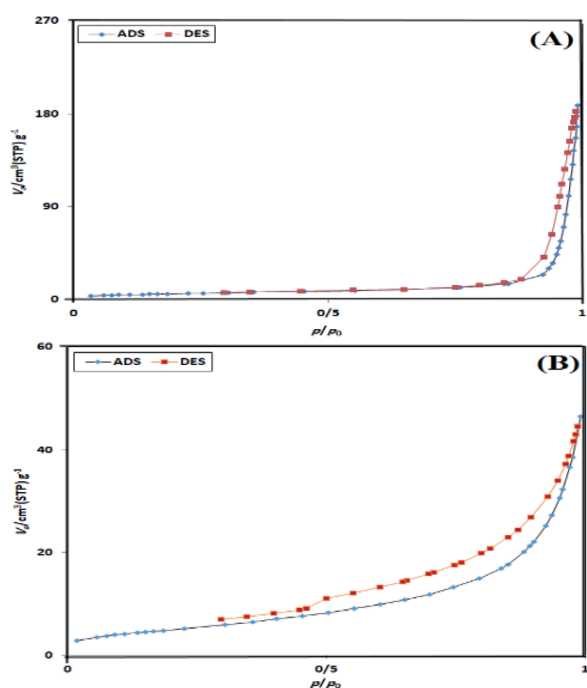
Fig. 7 The TGA curve for Alg–PSSA-*co*-ACA@Ni.

Fig. 8 N$_2$ adsorption–desorption isotherms of porous Alg–PSSA-*co*-ACA (A) and Alg–PSSA-*co*-ACA@Ni (B).

detected around the Ni NPs. In the prepared catalyst, the porous Alg–PSSA-*co*-ACA can play the role of both reducing and capping agent. In addition, the deposition of the Ni NPs was verified using EDX analysis. The HR-TEM image demonstrated the presence of Ni NPs along with the polymer in the catalyst without any noticeable change compared with that of the original one. In comparison with the fresh particles (Fig. 4A), the number of Ni NPs distributed on the mesoporous Alg–PSSA-*co*-ACA substrate seems to be reduced. This may be the reason for the reduction in the catalytic performance observed after recycling seven times. To obtain further confirmation for this claim, ICP-OES was performed on a sample of the supernatant after the particles were used for the seventh time, and it was revealed that 1.55 mmol g^{-1} of the Ni element existed in the sample. This means that the leaching of the Ni element from the catalytic system is an inevitable event, but this partial leaching does not have any significant effect on the catalytic performance.

The elemental composition of the Alg–PSSA-*co*-ACA@Ni was determined using energy dispersive X-ray spectroscopy (EDS) analysis and the presence of Na, O, S, C, N and Ni was confirmed (Fig. 5). From the weight percentage results of the EDS analysis of the prepared catalyst (Table 1), it can be understood that the successful polymerization of *para*-styrene sulfonamide (S: 30.41%) has been achieved. The presence of N (9.28%) and O (26.10) also confirmed the crosslinking of MBA and the polymerization of PSSA (Table 1). In addition, the elemental

Table 2 Textural parameters obtained from nitrogen adsorption studies

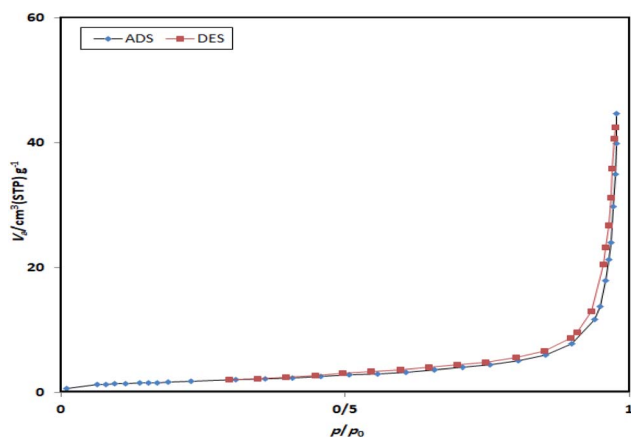| Sample	S_{BET} (m^2 g^{-1})	Pore diameter obtained using the BJH method (nm)	Pore volume (cm^3 g^{-1})
Alg–PSSA-*co*-ACA	22.41	25.55	0.27
Alg–PSSA-*co*-ACA@Ni	21.30	1.88	0.07

Fig. 9 N$_2$ adsorption–desorption isotherms of the recovered Alg–PSSA-*co*-ACA@Ni.

mapping exhibited the uniform distribution of all the elements, as shown in Fig. 6. In addition, the proper dispersion of the Ni NPs in the composite is obvious.

Fig. 7 shows the TGA curve of Alg–PSSA-*co*-ACA@Ni, in which a small weight loss from 30 to 100 °C can be observed, clearly related to the physically absorbed water. After this, the weight loss in the range of 230–320 °C clearly indicated the degradation of the Alg–PSSA-*co*-ACA groups.[41]

As shown in Fig. 8, according to the Brunauer–Emmett–Teller (BET) analysis, Alg–PSSA-*co*-ACA (Fig. 8A) and Alg–PSSA-*co*-ACA@Ni (Fig. 8B) showed a typical type IV isotherm with type H3 hysteresis (defined by IUPAC).[42] The results of the N$_2$-adsorption and desorption isotherms of Alg–PSSA-*co*-ACA and Alg–PSSA-*co*-ACA@Ni clearly demonstrated the immobilization of Ni NPs significantly reduces the pore diameter, pore volume and specific surface area (Table 2).

The N$_2$ adsorption–desorption isotherms of the seventh reused catalyst (Fig. 9) were measured in order to determine the textural properties. It can be seen from Fig. 9 that the reused catalyst shows a typical type IV isotherm with type H3 hysteresis (defined by IUPAC) and is identified as a mesoporous material.[42] The N$_2$ adsorption–desorption isotherms of the reused catalyst indicate that there is no obvious change in the catalytic composition after the reaction. The changes associated with the textural properties of the catalyst when reused for the seventh time could be due to the fact that the reactants were distributed inside the Alg–PSSA-*co*-ACA@Ni pores during the reaction (pore volume = 0.05 cm^3 g^{-1}, S_{BET} = 6.41 m^2 g^{-1}).

3.2. Catalytic tests

The catalytic activity of Alg–PSSA-*co*-ACA@Ni in the model reaction (iodobenzene, benzohydrazide and *tert*-butyl isocyanide) is presented in Table 3. At first, the protocol was optimized for the amount of the Alg–PSSA-*co*-ACA@Ni catalyst.

Table 3 Optimization of the reaction conditions[a]
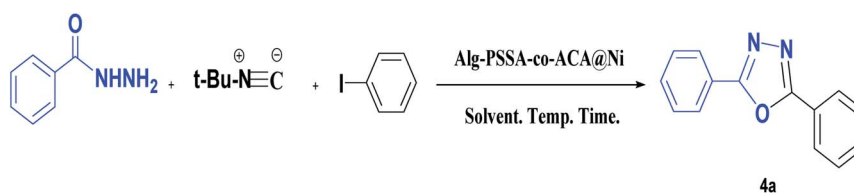
Entry	Cat. amount (mol%)	Solvent	T (°C)	Time (h)	Yield[b] (%)
1	1	EtOH	Reflux	2	58
2	1.5	EtOH	Reflux	2	75
3	**1.5**	**H$_2$O : EtOH (1 : 1)**	**Reflux**	**1**	**94**
4	3	H$_2$O : EtOH (1 : 1)	Reflux	1	94
5	1.5	H$_2$O : CH$_3$CN (1 : 1)	Reflux	1	79
6	1.5	H$_2$O : DMF (1 : 1)	Reflux	1	85
7	1.5	Solvent-free	(80 °C)	5	45
8	1.5	Toluene	Reflux	4	55
9	1.5	H$_2$O : EtOH (1 : 1)	(60 °C)	1	75
10	1.5	H$_2$O : EtOH (1 : 1)	Reflux	4	50[c]
11	100 mg	H$_2$O : EtOH (1 : 1)	Reflux	12	65[d]
12	9 mg	H$_2$O : EtOH (1 : 1)	Reflux	1	0[e]
13	9 mg	H$_2$O : EtOH (1 : 1)	Reflux	1	0[f]
14	9 mg	H$_2$O : EtOH (1 : 1)	Reflux	1	20[g]

[a] Reaction conditions: aryl iodide (1 mmol), benzohydrazide (1 mmol), *tert*-butyl isocyanide (1.5 mmol), KHCO$_3$ (1 mmol), and Alg–PSSA-*co*-ACA@Ni (1.5 mol%, 9 mg) were stirred in H$_2$O : EtOH (1 : 1, 2 mL) under reflux conditions. [b] Isolated pure yield. [c] The reaction was examined in the absence of a base. [d] The reaction was examined in the presence of Ni NPs. [e] The reaction was examined in the presence of Alg–PSSA-*co*-ACA. [f] The reaction was examined in the presence of SiO$_2$@Alg–PSSA-*co*-ACA. [g] The reaction was examined in the presence of NiCl$_2$.

Table 4 A comparison study of the catalytic efficiency of a variety of catalysts with different surface modifications

Catalyst	Yield of run 1 (%)	Yield of run 7 (%)	Time (h)
Alg@Ni	53	—	1
Alg–ACA@Ni	58	52	1
PSSA-*co*-ACA@Ni	90	75	1
Alg–PSSA-*co*-ACA@Ni	**94**	**84**	**1**

As the amount of catalyst increased (entries 1 and 2), the yield of the product increased rapidly in 1.5 mol% of the prepared catalyst (entry 2) but after the reaction it was independent of the amount of catalyst (entry 4). Then, the reaction was checked at several different temperatures, and in the presence of bases and various solvents. According to the catalytic results in different solvents (entries 4–8), in a mixture of EtOH : H_2O (1 : 1) the highest reactivity was observed. For optimization of the temperature (entry 9), the best result was observed under reflux conditions. Afterwards, by investigating the effect of bases on the reaction progress, it was observed that the reaction reached a 94% yield after 1 h with $KHCO_3$. Other inorganic and organic bases also showed good yields (NaOAc, NaOH, K_2CO_3, $KHCO_3$ and Et_3N). However, in the absence of a base, the yield was very low (entry 10). According to Table 1, the optimized reaction conditions are Alg–PSSA-*co*-ACA@Ni (1.5 mol%, 9 mg) using

1 mmol of $KHCO_3$ as the base in H_2O : EtOH (2 mL, 1 : 1) under reflux conditions (entry 3). As shown in Table 3, to reveal the importance of the porous Alg–PSSA-*co*-ACA in the catalyst, the Ni NPs only were also applied under the same conditions. As can be detected in Table 3 (entry 11), the obtained reaction yield was reduced after removing the porous Alg–PSSA-*co*-ACA from the catalytic system. Moreover, as the Ni NPs are the main catalytic site for this catalytic system it is estimated that by removing the Ni NPs from the catalytic system, the synthesis of the desired product did not occur (entries 12 and 13). On the other hand, the influence of $NiCl_2$ was also investigated and a low yield was obtained (entry 14). It is worth noting that a similar reaction in the presence of $NiCl_2$ and polysulfonamide with sodium borohydride failed to proceed.

To investigate the effect of the *para*-styrene sulfonamide ligand, another porous support was prepared in the absence of the *para*-styrene sulfonamide ligand, and the Ni NPs were immobilized onto the surface of the porous Alg–ACA (Table 4). The same model reaction was performed using the Alg–ACA@Ni catalyst and the results showed that in the absence of poly styrene sulfonamide the reaction did not precede very well and only 58% of the product was obtained. This reveals that poly-styrene sulfonamide on the surface of the catalyst significantly improved the catalytic activity of the immobilized Ni owing to the strong chelation of the supported ligand. Moreover, we also compared the catalytic performance of the Ni NPs immobilized on sodium alginate, porous Alg–ACA, PSSA-*co*-ACA and porous

Table 5 The substrate scope for the preparation of 1,3,4-oxadiazoles using different iodobenzenes[a]
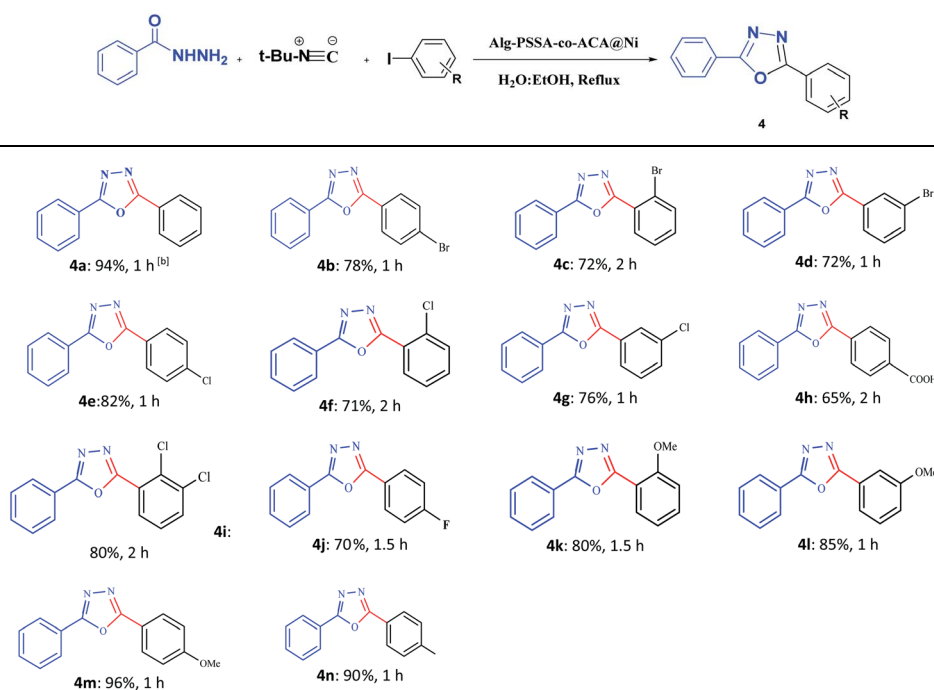
[a] Reaction conditions: aryl iodide (1 mmol), benzhydrazide (1 mmol), *tert*-butyl isocyanide (1.5 mmol), $KHCO_3$ (1 mmol), Alg–PBSA-*co*-ACA@Ni (1.5 mol%, 9 mg) were stirred in H_2O : EtOH (1 : 1, 2 mL) at reflux condition. *[b]* Isolated pure yield.
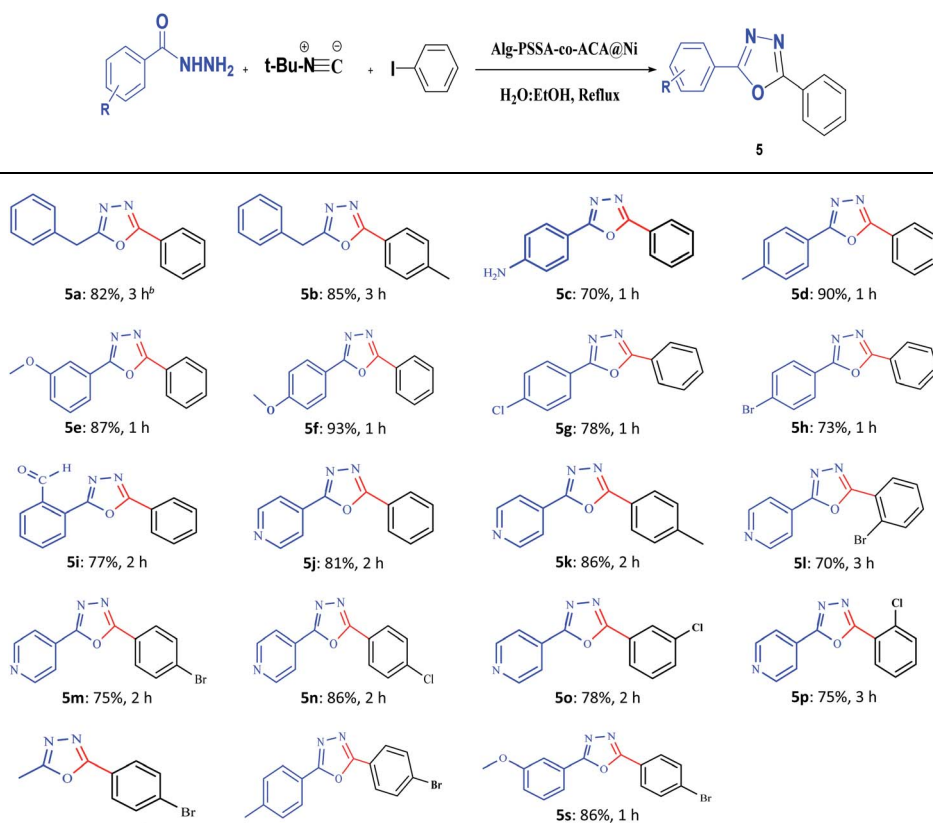
Alg–PSSA-*co*-ACA supports in both the fresh and recycled state under the same conditions (Table 4). The results show that the porous Alg–PSSA-*co*-ACA@Ni catalyst, in comparison with the others, is very suitable and efficient, leading to the preparation of 94% and 84% (after the 7th cycle) of the product in the fresh and recycled states, respectively, under the same conditions. In addition, as seen in Table 4, the presence of sodium alginate, acryl amide and polysulfonamide in the support matrix seems to be necessary for the further chemical stability of the catalyst compared to others in the recycled form, because after several runs, the amount of decomposition reduces, and the activity of the catalyst increases. To investigate the effect of chemical modification on the chelation between sodium alginate and Ni NPs, the loading amount of Ni was also characterized using ICP-OES (0.52 mmol g^{-1}) and it was observed that the loading of Ni had decreased. Thus, the significant role of the sodium alginate surface modification in the effective chelation of nickel NPs to the surface was proved.

After stabilizing the reaction conditions, as discussed in Table 5, the next endeavour was to ascertain their scope and generality over a broad range of substrates (Tables 5 and 6). We found that a variety of functionalized 1,3,4-oxadiazoles are accessible in good to excellent yields using this method. With regard to the scope of the aryl iodides, electron-withdrawing substituted aryl iodides such as *p*-Br, *o*-Br, *m*-Br, *p*-chloro, *m*-chloro, *o*-chloro, *p*-F, 2,3-Cl$_2$ and *p*-COOH (**4b–j**), electron-donating aryl iodides such as *p*-OCH$_3$, *o*-CH$_3$, *m*-OCH$_3$, *p*-CH$_3$ (**4k–n**) and sterically hindered aryl iodides (**4c, 4f, 4i, 4k**) are all good substrates. Iodobenzenes bearing electron-donating substituents gave the desired products in better yields as compared to electron-withdrawing aryl iodides. Moreover, this condition was assessed using a wide range of aryl iodides containing substituents in the *ortho* position (*e.g.*, OMe, Cl, Br) (**4c, 4f, 4k**), leading to moderate yields (Table 5).

The current study was extended to benzhydrazide derivatives using the optimized reaction conditions (Table 6). It was observed that various substituted benzhydrazides, including 2-phenylacetohydrazide (**5a–b**), benzhydrazides carrying –NH$_2$, –CH$_3$, and –OCH$_3$ (**5c–f**), and electron-withdrawing substituents such as pyridine, –Cl, –Br and formyl (**5g–k**) reacted successfully in good yields under the set reaction conditions. The yields for the benzhydrazide group are higher than those obtained for the electron-poor ones, probably owing to the stronger nucleophilicity. Interestingly, the reaction of the unreactive hydrazides

Table 6 Substrate scope for the preparation of 1,3,4-oxadiazoles using different benzhydrazides, iodobenzenes, and *tert*-butyl isocyanide under the optimized conditions[a]

5a: 82%, 3 h[b]   **5b**: 85%, 3 h   **5c**: 70%, 1 h   **5d**: 90%, 1 h

5e: 87%, 1 h   **5f**: 93%, 1 h   **5g**: 78%, 1 h   **5h**: 73%, 1 h

5i: 77%, 2 h   **5j**: 81%, 2 h   **5k**: 86%, 2 h   **5l**: 70%, 3 h

5m: 75%, 2 h   **5n**: 86%, 2 h   **5o**: 78%, 2 h   **5p**: 75%, 3 h

5s: 86%, 1 h

[a] Reaction conditions: aryl iodide (1 mmol), benzhydrazide (1 mmol), *tert*-butyl isocyanide (1.5 mmol), KHCO$_3$ (1 mmol), and Alg–PBSA-*co*-ACA@Ni (1.5 mol%, 9 mg) were stirred in H$_2$O : EtOH (1 : 1, 2 mL) under reflux conditions. [b] Isolated pure yield.

Table 7 Comparison of the present methodology with other reported catalysts for the synthesis of 2,5-diphenyl-1,3,4-oxadiazole (**4a**)

Entry	Conditions	Yield (%) [ref.]
1	PdCl$_2$ (0.0125 mmol), DPPP (0.025 mmol), NaOAc (1 mmol), DMF, 130 °C, 3 h	76 (ref. 10)
2	Cu(OTf)$_2$ (10 mol%), CsCO$_3$, DMF, 110 °C, *N*-arylidenearoylhydrazide (1 mmol), 16 h	85 (ref. 7)
3	*N*-acyl-*N'*-aryliden-hydrazines (0.5 mmol), Dess–Martin periodinane (0.5 g), CH$_2$Cl$_2$, 4 h	92 (ref. 43)
4	Benzaldehyde (1 mmol), benzhydrazide (1 mmol), I$_2$ (1.2 mmol), K$_2$CO$_3$ (3 mmol), EtOH, reflux temperature, 3 h	76 (ref. 6)
5	Alg–PBSA-*co*-ACA@Ni (1.5 mol%, 9 mg), KHCO$_3$ (1 mmol), H$_2$O : EtOH, reflux conditions, 1 h	94 [this work]

with the unreactive aryl iodide led to the desired product in a good yield (**5l–p**). It should be noted that the corresponding products were synthesized in good yields with the isomeric electron-deficient aryliodide: *o*-, *m*-, and *p*-chloro iodobenzene (**5n–p**). The longest reaction time was observed for the *o*-chloro benzhydrazide because of the electron-withdrawing effect of the chloro group and also the anchimeric resistance (steric hindrance). Moreover, the desired product was synthesized in good yields using acetohydrazide, *p*-toluoylhydrazide and *m*-anisohydrazide with *p*-bromoiodobenzene (**5q–s**). It is noteworthy that the reaction is highly regioselective as no regioisomeric chloro or bromo cyclization product could be detected. The products were characterized using physical and spectral (infrared spectroscopy, NMR, and mass spectrometry) data.

As revealed from the previously published literature and according to Table 6, in order to synthesize 2,5-diphenyl-1,3,4-oxadiazole, different conditions have been investigated (entries 1–4). As shown in this table and using the previously described method, all of the requested products were obtained in high yields during short reaction times (entry 5). The catalyst is an eco-friendly material owing to the fact that it is composed of sodium alginate and poly (*p*-styrene sulfonamide). Moreover, as evident from Table 7, when polystyrene sulfonamide and sodium alginate are present in the support matrix, they enable the greater chemical stability of the catalyst owing to the fact that even after several runs the catalyst activity is not

significantly decreased (yields of 94%, 94%, 92%, 90%, 88%, 87% and 84% are observed).

A plausible reaction pathway has been suggested in Scheme 3. The oxidative addition of aryl halides to the Ni(0) catalyst facilitates the formation of the palladium complex **A**, followed by insertion to obtain the nickel(II) species **B**. Then, benzhydrazides are added to intermediate **B**, with the assistance of KHCO$_3$, to form intermediate **C**. Finally, owing to the loss of the *tert*-butylamine and the cyclization of intermediate **D**, the desired product is produced (Scheme 3).[10]

3.3. Reusability study

As the reusability of any catalyst is a key factor for determining its commercial applicability, the reusability and recovery of the catalyst were tested by studying the reaction of iodobenzene, benzohydrazide and *tert*-butyl isocyanide, as model substrates. As expected, the catalyst illustrated a desirable reusability with a negligible reduction in its activity (Fig. 10, yields of 94%, 92%, 90%, 88%, 87% and 84 are observed). It could be separated from the reaction mixture by centrifugation, and was then washed with ethanol, and reused in the forthcoming catalytic reactions. In this research, we also report the amount of Ni that has leached from the NPs in the model reaction by checking the Ni loading amount before and after the recycling of the catalyst using the ICP-OES technique. It was observed that the amount of Ni in the fresh catalyst and the recycled catalyst after
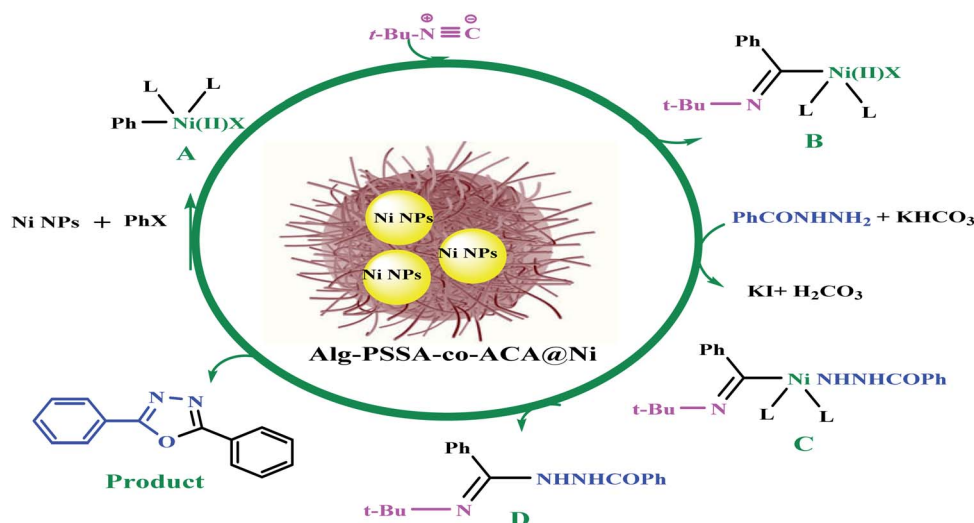
Scheme 3 The suggested mechanism for the synthesis of 1,3,4-oxadiazoles using Alg–PSSA-*co*-ACA@Ni.
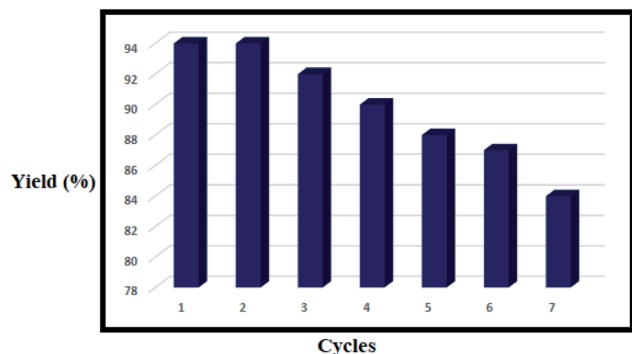
Fig. 10 Recycling of Alg–PSSA-co-ACA@Ni for the synthesis of 2,5-diphenyl-1,3,4-oxadiazole (**4a**).

recycling seven times was 1.60 and 1.55 mmol g^{-1}, respectively. Therefore, it can be stated that the nickel species remain active in the catalytic procedure owing to the excellent complexation of the amide, sulfonamide, carboxylate and hydroxyl groups. This result also demonstrated that the amount of nickel that leached from the catalyst was low.

4. Conclusions

The purpose of the current study was to design a novel catalyst consisting of Ni decorated on a porous support containing Alg–PSSA–ACA and to evaluate its catalytic activity for the green synthesis of 1,3,4-oxadiazoles. Alg–PSSA-co-ACA@Ni has been developed as a highly active and recoverable heterogeneous catalyst for the preparation of diverse functionalized 1,3,4-oxadiazoles. The results illustrate that the amphiphilicity and high metal loading result in the high performance of the catalyst. Hence, because of these great features, we recommend Alg–PSSA-co-ACA@Ni as a robust and promising candidate for this important type of chemical conversion.

Conflicts of interest

The authors listed in this article have no conflict of interests.

Acknowledgements

References

1 H. Khalilullah, M. J. Ahsan, M. Hedaitullah, S. Khan and B. Ahmed, 1,3,4-Oxadiazole: a biologically active scaffold, *Mini-Rev. Med. Chem.*, 2012, **12**, 789–801.

2 N. D. James and J. W. Growcott, Zibotentan endothelin ETA receptor antagonist oncolytic, *Drugs Future*, 2009, **34**, 624–633.

3 V. Summa, A. Petrocchi, F. Bonelli, B. Crescenzi, M. Donghi, M. Ferrara, F. Iore, C. Gardelli, O. Gonzalez Paz, D. J. Hazuda, P. Jones, O. Kinzel, R. Laufer, E. Monteagudo, E. Muraglia, E. Nizi, F. Orvieto, P. Pace, G. Pescatore, R. Scarpelli, K. Stillmock, M. V. Witmer and M. Rowley, Discovery of raltegravir, a potent, *J. Med. Chem.*, 2008, **51**, 5843–5855.

4 Q. H. Gao, S. Liu, X. Wu, J. J. Zhang and A. X. Wu, *Org. Lett.*, 2015, **17**, 2960–2963.

5 M. Al-Talib, H. Tashtoush and N. Odeh, *Synth. Commun.*, 1990, **20**, 1811–1817.

6 G. Majji, S. K. Rout, S. Guin, A. Gogoi and B. K. Patel, *RSC Adv.*, 2014, **4**, 5357–5362.

7 S. Guin, T. Ghosh, S. K. Rout, A. Banerjee and B. K. Patel, *Org. Lett.*, 2011, **13**, 5976–5979.

8 T. Kawano, T. Yoshizumi, K. Hirano, T. Satoh and M. Miura, *Org. Lett.*, 2009, **11**, 3072–3075.

9 C. Xu, F. C. Jia, Q. Cai, D. K. Li, Z. W. Zhou and A. X. Wu, *Chem. Commun.*, 2015, **51**, 6629–6632.

10 X.-Y. Fan, X. Jiang, Y. Zhang, Z.-B. Chen and Y.-M. Zhu, *Org. Biomol. Chem.*, 2015, **13**, 10402–10408.

11 R. Poupart, D. Grande, B. Carbonnier and B. Droumaguet, *Prog. Polym. Sci.*, 2019, **96**, 21–42.

12 Z. B. Shifrina, V. G. Matveeva and L. M. Bronstein, *Chem. Rev.*, 2020, **120**, 1350–1396.

13 S. Alizadeh and D. Nematollahi, *J. Am. Chem. Soc.*, 2017, **139**, 4753–4761.

14 S. Babaee, M. Zarei, M. A. Zolfigol, S. Khazalpour, M. Hasani, U. Rinner, R. Schirhagl, N. Norouzi and S. Rostamnia, *RSC Adv.*, 2021, **11**, 2141–2157.

15 M. Zhang, L. He, T. Shi and R. Zha, *Chem. Mater.*, 2018, **30**, 7391–7412.

16 K. Kim, S. Baek, J. Rho and H. Lee, *ACS Appl. Mater. Interfaces*, 2019, **11**, 26109–26115.

17 S. Khalid, G. Abbas, M. Hanif, S. Shah, S. Nisar, H. Shah, A. Jalil, M. Yaqoob, N. Ameer and A. Anum, *Int. J. Biol. Macromol.*, 2020, **164**, 2691–2700.

18 H. Veisi, Z. Joshani, B. Karmakar, T. Tamoradi, M. M. Heravi and J. Gholami, *Int. J. Biol. Macromol.*, 2021, **172**, 104–113.

19 R. Ghorbani-Vaghei, H. Veisi, M. HajiAliani, P. Mohammadi and B. Karmakar, *J. Mol. Liq.*, 2020, **327**, 114868–114876.

20 F. Bayat, A. R. Karimi and T. Adimi, *Int. J. Biol. Macromol.*, 2020, **159**, 598–606.

21 A. Maleki, R. Firouzi-Haji and Z. Hajizadeh, *Int. J. Biol. Macromol.*, 2018, **116**, 320–326.

22 A. Maleki, V. Eskandarpour, J. Rahimi and N. Hamidi, *Carbohydr. Polym.*, 2019, **208**, 251–260.

23 H. V. Saether, H. K. Holme, G. Maurstad, O. SmidsrØd and B. T. Stokke, *Carbohydr. Polym.*, 2008, **74**, 813–821.

24 S. Hua and A. Wang, *Carbohydr. Polym.*, 2009, **75**, 79–84.

25 L. Yang, J. Guo, J. Wu, Y. Yang, S. Zhang, J. Song, Q. An and Y. Gong, *RSC Adv.*, 2017, **7**, 50626–50633.

26 N. Işıklan and F. Kurşun, *Polym. Bull.*, 2013, **70**, 1065–1084.

27 M. M. Soledad Lencina, Z. Iatridi, M. A. Villar and C. Tsitsilianis, *Eur. Polym. J.*, 2014, **61**, 33–44.

28 Y. Kitamura, M. Kandeel, T. Kondo, A. Tanaka, Y. Makino, N. Miyamoto, A. Shibata, M. Ikeda and Y. Kitade, *Bioorg. Med. Chem. Lett.*, 2020, **30**, 127637–127657.

29 (*a*) S. Alavinia and R. Ghorbani-Vaghei, *J. Phys. Chem. Solids*, 2020, **146**, 109573–109584; (*b*) F. Hamidi Dastjerdi, R. Ghorbani-Vaghei and S. Alavinia, *Catal. Lett.*, 2020, **150**, 3514–3522; (*c*) S. Alavinia, R. Ghorbani-Vaghei, J. Rakhtshah, J. Yousefi Seyf and I. Ali Arabian, *Appl. Organomet. Chem.*, 2020, **34**, e5449; (*d*) S. Alavinia and R. Ghorbani-Vaghei, *New J. Chem.*, 2020, **44**, 13062–13073; (*e*) S. Solgi, R. Ghorbani-Vaghei and S. Alavinia, *J. Porous Mater.*, 2021, **28**, 289–298; (*f*) N. Shekarlab, R. Ghorbani-Vaghei and S. Alavinia, *J. Organomet. Chem.*, 2021, **949**, 121971; (*g*) A. Rahimi, R. Ghorbani-Vaghei and S. Alavinia, *J. Porous Mater.*, 2021, 1–11, DOI: 10.1007/s10934-021-01104-1; (*h*) S. Zafari, R. Ghorbani-Vaghei and S. Alavinia, *Mater. Chem. Phys.*, 2021, **270**, 124840; (*i*) N. Shekarlab, R. Ghorbani-Vaghei and S. Alavinia, *Appl. Organomet. Chem.*, 2020, **34**, e5918.

30 (*a*) K. Katagiri, T. Sakai, M. Hishikawa, H. Masu, M. Tominaga, K. Yamaguchi and I. Azumaya, *Cryst. Growth Des.*, 2014, **14**, 199–206; (*b*) M. Roca, R. L. Althaus and M. P. Molina, *Food Chem.*, 2013, **136**, 376–383.

31 R. Ghorbani-Vaghei and N. Sarmast, *Can. J. Chem.*, 2017, **95**, 1073–1084.

32 (*a*) R. Ghorbani-Vaghei, S. Alavinia, Z. Merati and V. Izadkhah, *Appl. Organomet. Chem.*, 2018, **32**, e4127; (*b*) A. Fatehi, R. Ghorbani-Vaghei, S. Alavinia and J. Mahmoodi, *ChemistrySelect*, 2020, **5**, 944; (*c*)

R. Ghorbani-Vaghei, S. Alavinia and N. Sarmast, *Appl. Organomet. Chem.*, 2018, **32**, e4038.

33 W. Stöberand and A. Fink, *J. Colloid Interface Sci.*, 1968, **26**, 62–69.

34 S. Khan, A. Ghatak and S. Bhar, *Tetrahedron Lett.*, 2015, **56**, 2480–2487.

35 A. G. Ibrahim, A. Z. Sayed, H. A. El-Wahab and M. M. Sayah, *Am. J. Polym. Sci. Technol.*, 2019, **5**, 55–62.

36 J. Lin, H. Huang, M. Wang and J. Deng, *Polym. Chem.*, 2016, **7**, 1675–1681.

37 M. R. Ahghari, V. Soltaninejad and A. Maleki, *Sci. Rep.*, 2020, **10**, 12627.

38 T. A. Saleh, A. M. Elsharif, S. Asiri, A. R. Mohammed and H. Dafalla, *Environ. Nanotechnol. Monit. Manag.*, 2020, **14**, 100302.

39 A. Ahmed, F. Mohamed, A. M. Elzanaty and O. F. Abdel-Gawad, *Int. J. Biol. Macromol.*, 2021, **167**, 766–776.

40 L. Jia, D. Wang, L. Liu, S. Zhang and T. Xu, *Des. Monomers Polym.*, 2014, **17**, 425–429.

41 Z. Bahrami, A. Akbari and B. Eftekhari-Sis, *Int. J. Biol. Macromol.*, 2019, **129**, 187–197.

42 S. W. Sing and W. Kenneth, *Adsorpt. Sci. Technol.*, 2004, **22**, 773–782.

43 C. Dobrotă, C. C. Paraschivescu, I. Dumitru, M. Matache, I. Baciu and L. L. Ruță, *Tetrahedron Lett.*, 2009, **50**, 1886–1888.